Fatigue Evaluation of Reinforced and Unreinforced Hand Holes in High-Mast Lighting Towers

Final Report
September 2021

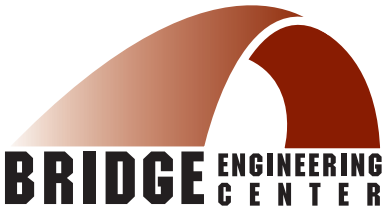

IOWA STATE UNIVERSITY
Institute for Transportation

Sponsored by
Iowa Department of Transportation
(InTrans Project 17-597)

About the Bridge Engineering Center

The mission of the Bridge Engineering Center (BEC) is to conduct research on bridge technologies to help bridge designers/owners design, build, and maintain long-lasting bridges.

About the Institute for Transportation

The mission of the Institute for Transportation (InTrans) at Iowa State University is to save lives and improve economic vitality through discovery, research innovation, outreach, and the implementation of bold ideas.

Iowa State University Nondiscrimination Statement

Iowa State University does not discriminate on the basis of race, color, age, ethnicity, religion, national origin, pregnancy, sexual orientation, gender identity, genetic information, sex, marital status, disability, or status as a US veteran. Inquiries regarding nondiscrimination policies may be directed to the Office of Equal Opportunity, 3410 Beardshear Hall, 515 Morrill Road, Ames, Iowa 50011, telephone: 515-294-7612, hotline: 515-294-1222, email: eooffice@iastate.edu.

Disclaimer Notice

The contents of this report reflect the views of the authors, who are responsible for the facts and the accuracy of the information presented herein. The opinions, findings and conclusions expressed in this publication are those of the authors and not necessarily those of the sponsors.

The sponsors assume no liability for the contents or use of the information contained in this document. This report does not constitute a standard, specification, or regulation.

The sponsors do not endorse products or manufacturers. Trademarks or manufacturers' names appear in this report only because they are considered essential to the objective of the document.

Iowa DOT Statements

Federal and state laws prohibit employment and/or public accommodation discrimination on the basis of age, color, creed, disability, gender identity, national origin, pregnancy, race, religion, sex, sexual orientation or veteran's status. If you believe you have been discriminated against, please contact the Iowa Civil Rights Commission at 800-457-4416 or Iowa Department of Transportation's affirmative action officer. If you need accommodations because of a disability to access the Iowa Department of Transportation's services, contact the agency's affirmative action officer at 800-262-0003.

The preparation of this report was financed in part through funds provided by the Iowa Department of Transportation through its "Second Revised Agreement for the Management of Research Conducted by Iowa State University for the Iowa Department of Transportation" and its amendments.

The opinions, findings, and conclusions expressed in this publication are those of the authors and not necessarily those of the Iowa Department of Transportation.

Technical Report Documentation Page

1. Report No.	2. Government Accession No.	3. Recipient's Catalog No.
InTrans Project 17-597		

4. Title and Subtitle	5. Report Date
Fatigue Evaluation of Reinforced and Unreinforced Hand Holes in High-Mast Lighting Towers	September 2021
	6. Performing Organization Code

7. Author(s)	8. Performing Organization Report No.
Alice Alipour (orcid.org/0000-0001-6893-9602) and Li-Wei Tsai (orcid.org/0000-0002-0343-1979)	InTrans Project 17-597

9. Performing Organization Name and Address	10. Work Unit No. (TRAIS)
Bridge Engineering Center Iowa State University 2711 South Loop Drive, Suite 4700 Ames, IA 50010-8664	11. Contract or Grant No.

12. Sponsoring Organization Name and Address	13. Type of Report and Period Covered
Iowa Department of Transportation 800 Lincoln Way Ames, IA 50010	Final Report
	14. Sponsoring Agency Code 17-SPRO-018

15. Supplementary Notes

Visit https://intrans.iastate.edu for color pdfs of this and other research reports.

16. Abstract

High-mast lighting towers have been widely used to illuminate large areas such as freeways, airports, stadiums, and sports facilities throughout the nation and across the world. A hand hole is commonly found near the base of these structures as the access to the electrical wires inside the structure. The current American Association of State Highway and Transportation Officials (AASHTO) design standard of high-mast lighting towers with a tube diameter larger than 30 in. and sign and signal support structures requires that the width of the hand hole shall not be greater than 40% of the tube diameter. It also specifies that when calculating the nominal stress at the hand hole, it should be magnified by a stress concentration of 4.0. However, this design standard is actually difficult to follow in some pole structures with a small diameter.

A limited review of the currently fabricated structures showed that high-mast lighting towers in the range of 55 to 100 ft in height are most affected, where openings as large as 87% of the pole diameter have been used. The application of the stress concentration factor of 4.0 on these poles results in either increasing the thickness of the tubes or increasing the dimeter of the tube, which leads to a much more expensive pole and overall luminaire system.

The goal of the research is to identify the fatigue resistance of high-mast pole specimens with different opening ratios of the hand hole. Particularly, this study included the following objectives:

- Conduct fatigue experiments on two types of high-mast pole specimens with opening ratios of 46% and 54% and identify their fatigue resistance
- Build finite element models for pole specimens with different opening ratios to observe the change of the stress response at the pole base
- Use the results from the fatigue experiment and finite element analysis to study the influence of the opening ratio on the fatigue resistance of a high-mast lighting tower

17. Key Words	18. Distribution Statement
fatigue performance—finite element analysis—full-scale experiments—high-mast lighting towers—light pole hand holes	No restrictions.

19. Security Classification (of this report)	20. Security Classification (of this page)	21. No. of Pages	22. Price
Unclassified.	Unclassified.	49	NA

Form DOT F 1700.7 (8-72) **Reproduction of completed page authorized**

FATIGUE EVALUATION OF REINFORCED AND UNREINFORCED HAND HOLES IN HIGH-MAST LIGHTING TOWERS

Final Report
September 2021

Principal Investigator
Alice Alipour, Associate Professor
Bridge Engineering Center, Iowa State University

Co-Principal Investigator
Brent Phares, Bridge Research Engineer
Bridge Engineering Center, Iowa State University

Research Assistant
Li-Wei Tsai

Authors
Alice Alipour and Li-Wei Tsai

Sponsored by
Iowa Department of Transportation
(InTrans Project 17-597)

Preparation of this report was financed in part
through funds provided by the Iowa Department of Transportation
through its Research Management Agreement with the
Institute for Transportation

A report from
Bridge Engineering Center
Iowa State University
2711 South Loop Drive, Suite 4700
Ames, IA 50010-8664
Phone: 515-294-8103 / Fax: 515-294-0467
https://intrans.iastate.edu

TABLE OF CONTENTS

LIST OF FIGURES

LIST OF TABLES

ACKNOWLEDGMENTS

The authors would like to thank the Iowa Department of Transportation (DOT) for sponsoring this research using state planning and research funds and the technical advisory committee (TAC) members: Harold Adcock and Michael Jorgensen from Iowa DOT, Hannah Cheng from NJ DOT, and Carl Macchietto from Valmont Industries.

EXECUTIVE SUMMARY

High-mast lighting towers are widely used to illuminate large areas such as freeways, airports, stadiums, and sports facilities throughout the nation and across the world. Generally, these structures are composed of a high-mast tapered pole and luminaire assembly installed at the tip of the pole. Luminaire systems are installed at a high elevation to maximize the illuminated area. Typically, the height of these structures can be from 50 ft to 150 ft. However, because of the slenderness and the large mass of the structure itself, a high stress level usually appears at the base part of the structure while the structure is vibrating. At the same time, low structural damping causes stress cycles at the base part of the structure to easily accumulate, and eventually fatigue damage is created on the structures.

A hand hole is commonly found near the base of these structures as the access to the electrical wires inside the structure. The current American Association of State Highway and Transportation Officials (AASHTO) design standard of high-mast lighting towers with a tube diameter larger than 30 in. and sign and signal support structures requires that the width of the hand hole shall not be greater than 40% of the tube diameter. It also specifies that when calculating the nominal stress at the hand hole, it should be magnified by a stress concentration of 4.0. However, this design standard is actually difficult to follow in some pole structures with a small diameter.

A limited review of the currently fabricated structures showed that high-mast lighting towers in the range of 55 to 100 ft in height are most affected, where openings as large as 87% of the pole diameter have been used. The application of the stress concentration factor of 4.0 on these poles results in either increasing the thickness of the tubes or increasing the dimeter of the tube, which leads to a much more expensive pole and overall luminaire system.

The goal of the research was to identify the fatigue resistance of high-mast pole specimens with different opening ratios of the hand hole.

The findings of this study are as follows:

- First, the fatigue resistance of the base-to-tube connection decreased as the opening ratio of the hand hole increases. Specimen A had an opening ratio of 0.46, and the fatigue resistance of its base-to-tube connection was determined to be higher than Category E′ and possibly lower than Category E. Specimen B had an opening ratio of 0.54, and the fatigue resistance of its base-to-tube connection was determined to be near the lower limit of Category E′. From the parametric study, a slightly increasing trend of stress at the base-to-tube connection was found as the opening ratio increases. This could be the reason that fatigue resistance decreases at the base-to-tube connection.

- Second, the fatigue resistance of the hand-hole-to-tube connection might be higher than the base-to-tube connection, as no fatigue cracks were observed around both larger and smaller hand holes in both fatigue tests.

- Third, the location of fatigue cracks on a high-mast pole specimen might not completely relate to the stress response, as fatigue cracks were only observed at the base-to-tube connection. However, the stress response at the base-to-tube connection was lower than the stress response at the hand hole corners. There might be other factors such as the geometry near the discontinuities that determine where a fatigue crack will occur on a pole specimen.

1. INTRODUCTION

1.1. General Introduction

High-mast lighting towers are widely used to illuminate large areas such as freeways, airports, stadiums, and sports facilities throughout the nation and across the world. Generally, these structures are composed of a high-mast tapered pole and luminaire assembly installed at the tip of the pole. Luminaire systems are installed at a high elevation to maximize the illuminated area. Typically, the height of these structures can be from 50 ft to 150 ft. However, because of the slenderness and the large mass of the structure itself, a high stress level usually appears at the base part of the structure while the structure is vibrating. At the same time, low structural damping causes stress cycles at the base part of the structure to easily accumulate, and eventually fatigue damage is created on the structures.

Historically, failures and cracking of high-mast lighting towers have been frequently reported. In Iowa, a high-mast lighting tower placed along I-29 near Sioux City collapsed in 2003 within its five-year service life. After this failure, a statewide investigation was conducted in which cracks were found on more than 20 other high-mast lighting towers (Dexter 2004, Phares et al. 2007). In western Illinois, approximately 140 aluminum lighting poles collapsed during a 2003 winter storm (Caracoglia and Jones 2004). Phares et al. (2007) summarized most failure events in history in a table that showed that cracks on high-mast lighting towers were mostly found at the base-plate-to-tube connection, suggesting that fatigue damage can easily develop at locations with high stress levels. Also, all these instances showed the vulnerability of high-mast lighting towers to fatigue damage and the need to study their fatigue performance.

1.2. Wind Engineering of High-Mast Lighting Towers

Wind is believed to be a major source in causing the vibration of high-mast lighting towers. A few types of wind forces are suspected of inducing the vibration, which include buffeting wind force, vortex-shedding wind force, and truck-induced wind force. To understand wind-induced vibration, high-mast lighting towers in the field were monitored in several studies (Ahearn and Puckett 2010, Goode and van de Lindt 2006, Phares et al. 2007).

In Phares et al. (2007), two 150 ft high-mast lighting towers in Iowa were monitored. Strain gauges were installed around the base-to-tube connection and the hand hole corners to monitor the stress response during wind-induced vibrations. It was found that buffeting and vortex-shedding wind forces can induce high stress cycles at the base. Buffeting wind force can induce vibration in the along-wind direction. Higher wind speed can create larger buffeting wind force. The highest stress at the base was found to be induced by this type of wind force. Vortex-shedding wind force can induce vibration in the across-wind direction, which results from the vortices generated in the wake of the structure and usually happens at low wind speeds. From the monitoring data, the second-mode vortex-induced vibration was frequently observed at low wind speeds of 3–8 mph. The stress range during the vortex-induced vibration can be larger than the

constant amplitude fatigue limit (CAFL), which can possibly cause fatigue damage on the structure.

In Ahearn and Puckett (2010), two high-mast lighting towers in Wyoming were monitored. Accelerometers were installed at certain locations on the poles to detect vortex-induced vibration from different modes and truck-induced vibration. Strain gauges were installed at the base to record the stress response during the vibration. In this study, it was found that the third-mode vortex-induced vibration was frequently observed, and the stress range at the base was able to reach the CAFL during the vibration. It was also found that the acceleration results from the truck-induced wind force was quite small, which indicated truck-induced vibration might not be a concern for fatigue damage.

In these two studies, pluck tests were conducted to extract the dynamic property of the monitored structures. The monitored structures all showed a low damping ratio of the first mode around 0.5%, and the damping ratios of the rest modes were even lower. Low mechanical damping can make wind-induced vibration last longer, and fatigue damage will possibly accumulate faster.

To quantify the wind force on high-mast lighting towers, wind tunnel tests were conducted on scaled models to extract the aerodynamic and aeroelastic parameters. In Chang et al. (2014) and Phares et al. (2007), a high-mast lighting tower was modeled as a 12-sided cylinder. The wind tunnel tests included a static test to extract the drag and lift coefficients, a dynamic test to extract the vortex-shedding parameters, and a buffeting test to identify the buffeting indicial function. These identified parameters were later used to build a wind force equation, and a mathematical model was used to simulate the wind-induced response of the high-mast lighting tower.

In Luo et al. (2017), a scaled model of a 130 ft high lighting pole was tested in a wind tunnel. The coefficients to calculate the wind load in the along-wind and across-wind directions on the structure were identified. The aerodynamic instability of the structure was also examined through the wind tunnel tests.

1.3. Fatigue Performance of High-Mast Lighting Towers

The fatigue performance of high-mast lighting towers can be evaluated through conducting fatigue experiments. In Rios (2007) and Stam et al. (2011), 16-sided pole specimens without hand holes were tested. The fillet welded base-plate-to-tube connection was evaluated as less than Category E′, and the full-penetration welded base-plate-to-tube connection was evaluated as less than Category E.

In Roy et al. (2011), 16-sided pole specimens with hand holes were tested. At the base-plate-to-tube connection, the fillet welded type without backing ring was evaluated as Category E, and the fillet welded type with backing ring was evaluated as lying between Category E and Category D. The specimen reinforced by retrofit jacket exhibited a fatigue resistance in Category C. All fatigue cracks were found at the weld toe of the base-plate-to-tube connection or the weld toe of the backing ring. No fatigue cracks were discovered around the hand hole. At the hand-

hole-frame-to-tube connection, the fatigue resistance of a reinforced hand hole was predicted as Category D and an unreinforced hand hole was predicted as Category E′.

A hand hole is commonly found on a high-mast lighting tower to allow access to the electrical wires. However, a hand hole creates an irregular shape on the base part of a high-mast lighting tower, which results in stress concentration and a high stress level around the hand hole. Currently, there are few studies on the influence the hand hole on a high-mast lighting tower has on the structure's fatigue performance.

In Schlatter (2017), fatigue experiments were conducted on circular tube specimens with a hand hole to determine the fatigue resistance of the hand hole. The hand-hole-to-tube connection exhibited a fatigue resistance between Category D and Category C. A fatigue experiment was conducted by applying fatigue loading to bend the tube specimens. However, in reality, this type of deformation might not be like the deformation of a high-mast lighting tower with a hand hole during wind-induced vibration. Also, the tube specimens in this study did not have a base plate and a base-plate-to-tube connection, which was not like the base part of a real high-mast lighting tower. Thus, these fatigue test results cannot show the influence of the hand hole on the fatigue resistance of a high-mast lighting tower.

1.4. Research Objectives

According to American Association of State Highway and Transportation Officials (AASHTO) specifications (AASHTO 2015), the current design standard of high-mast lighting towers with a tube diameter larger than 30 in. and sign and signal support structures requires that the width of the hand hole shall not be greater than 40% of the tube diameter. It also specifies that when calculating the nominal stress at the hand hole, it should be magnified by a stress concentration of 4.0.

In Roy et al. (2011), mast arm specimens, which are composed of a horizontal arm and a vertical pole, and high-mast pole specimens were fatigue tested. The mast arm specimen has a hand hole on the base part of the vertical pole. Therefore, the geometry of the base part of the mast arm specimens was very similar to the base part of the high-mast pole specimens. The hand hole dimension on both specimens followed the current design standard. No fatigue cracks were found around the hand hole of the high-mast pole specimens; however, fatigue cracks were found on the corners of the hand hole on the mast arm specimens. This indicated the current design standard of the hand hole dimension might not be generally appropriate. Additionally, this design standard is actually difficult to follow in some pole structures with a small diameter.

A limited review of the currently fabricated structures showed that high-level luminaire structures in the range of 55 to 100 ft height are most affected, where openings as large as 87% of the pole diameter (or about 28% of the pole perimeter) have been used. In sign and signal support structures, poles of 10 in. diameter or less appear to be the most impacted. Unfortunately, there are a significant number of these structures in service and planned for future installation.

In other situations, multiple openings may be needed on a particular section that cumulatively exceeds 40% of the pole diameter. The application of the stress concentration factor of 4.0 on these poles results in either increasing the thickness of the tubes or increasing the dimeter of the tube, which results in requiring larger foundations and also additional thickness. In one example of the impact, the Oklahoma Department of Transportation (DOT) had poles with diameter of 7.8 in. that with a 4.69 in. hole resulted in a 60.2% opening. With the current standard, the poles need to be designed with a diameter of 11.72 in. This additional diameter would result in a much more expensive pole and overall luminaire system.

To propose a safer and more realistic design standard of the hand hole, research on the influence of the hand hole on the fatigue performance of high-mast lighting towers is needed. In this study, two different high-mast pole specimens with the same base-plate-to-tube connection but a different size of hand hole opening were tested. Static tests were first conducted on both specimens to see the difference of the stress response at the base part due to the different size of the hand hole opening. Fatigue tests were then conducted to determine the fatigue resistance of both specimens. To increase the efficiency of conducting fatigue tests, an experiment setup similar to the one used in Rios (2007) and Stam et al. (2011) was used to test the two specimens at the same time. Finally, additional finite element models with different opening ratios were built to conduct a parametric study. Based on the parametric study and the present fatigue experiment, the influence of the opening ratio on the fatigue resistance of a high-mast lighting tower was determined in this study.

1.5. Report Organization

This report is organized as follows:

- Chapter 2 describes the preliminary study of different types of high-mast pole specimens and the finite element analysis of the selected specimens
- Chapter 3 explains the fatigue experiment that includes the experiment setup, instrumentation, test procedures, and test results
- Chapter 4 shows the parametric study on the hand hole
- Chapter 5 presents the findings of this report and proposes future work

2. FINITE ELEMENT ANALYSIS

High-mast pole specimens with a hand hole have been fatigue tested in Roy et al. (2011). In this chapter, finite element models of the specimen Type X and Type XI in Roy et al. (2011) were built. To study the influence of the hand hole, the width of the opening of both initial specimens was increased to test another two specimens. Therefore, a total of four different pole specimen models were studied.

2.1. Model Description

In this section, four different high-mast pole specimen models were studied, which were named Specimen A, B, C, and D. All the specimen models were composed of a 19 ft 16-sided tube, a square top plate, and a circular base plate.

Specimen A followed the design details of specimen Type XI in Roy et al. (2011). There were eight bolt holes on the base plate. The base-to-tube connection used the full-penetration welded type and had a 2 in. backing ring inside the base. The opening of the hand hole of Specimen A was 11 in., which was equal to 45.8% of the tube diameter. Specimen B was almost identical to Specimen A but had a 13 in. opening, which was equal to 54.2% of the tube diameter. See the dimension details in Figure 2.1.

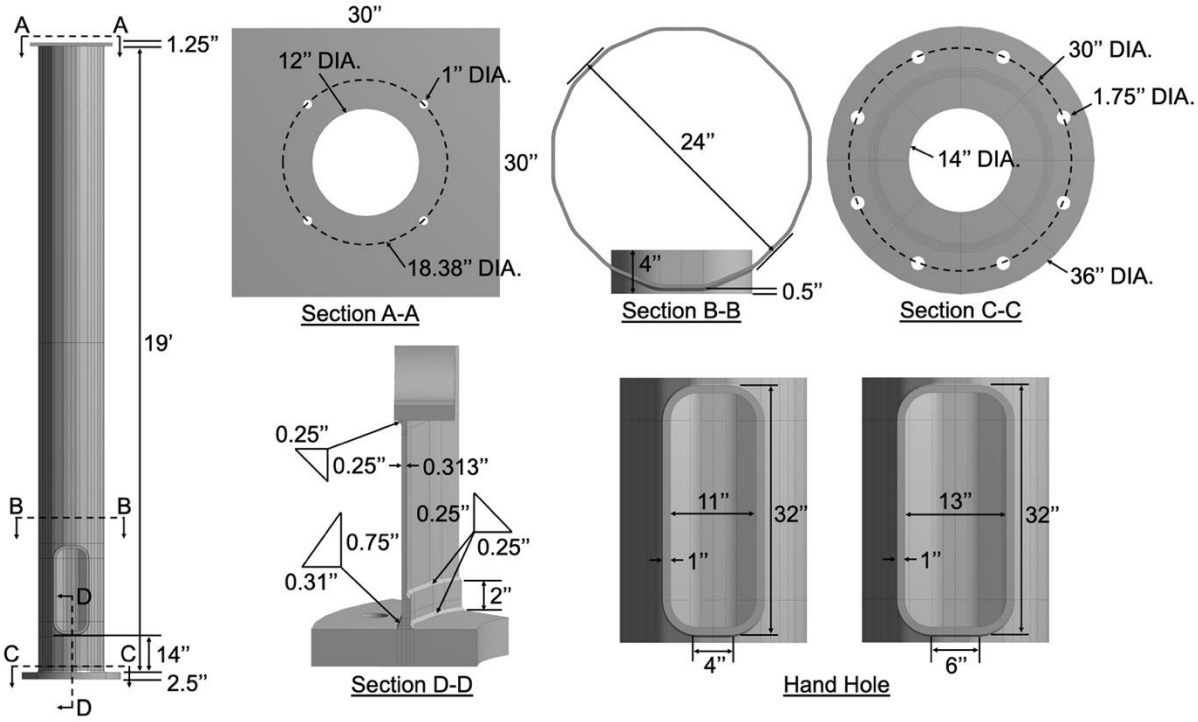

Figure 2.1. Dimension details of Specimens A and B

Specimen C followed the design details of specimen Type X in Roy et al. (2011). There were 16 bolt holes on the base plate. The base-to-tube connection selected was the fillet welded type with no backing ring inside the base. The opening of Specimen C was 11 in., which was equal to 45.8% of the tube diameter. Specimen D was almost identical to Specimen C but had a 13 in. opening, which was equal to 54.2% of the tube diameter. See the dimension details in Figure 2.2.

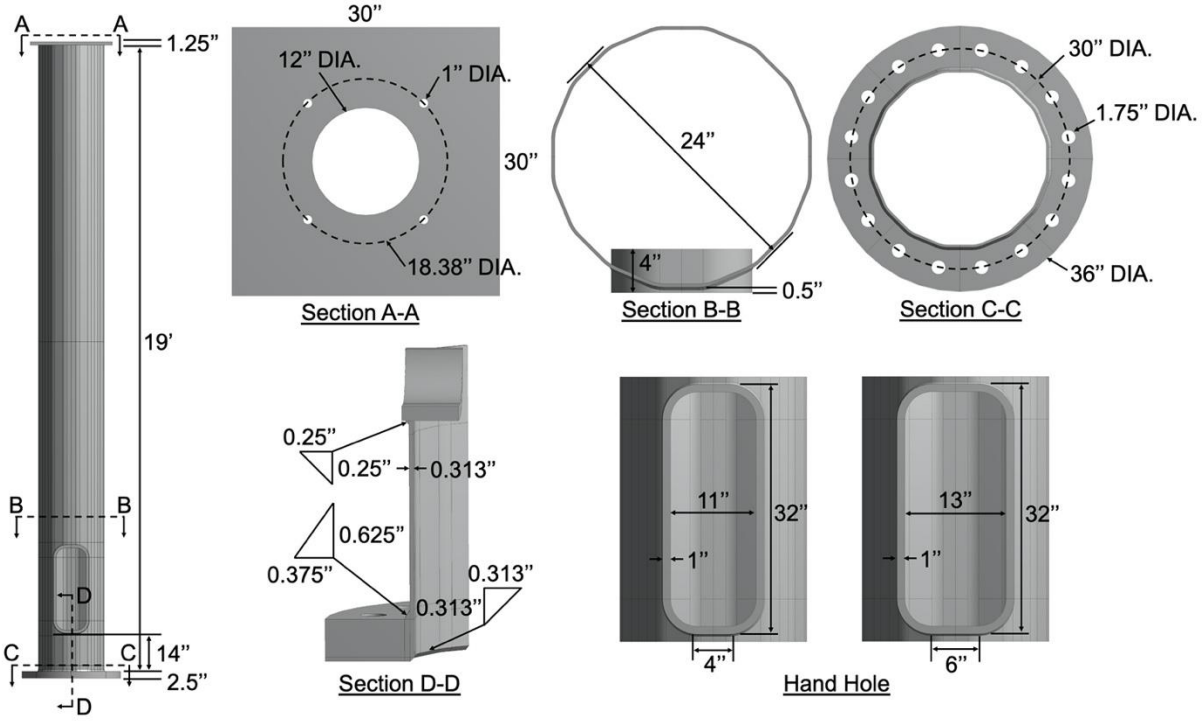

Figure 2.2. Dimension details of Specimens C and D

To make the connection at the base more like the real condition, a bolted connection and a solid foundation were also modeled (see Figure 2.3).

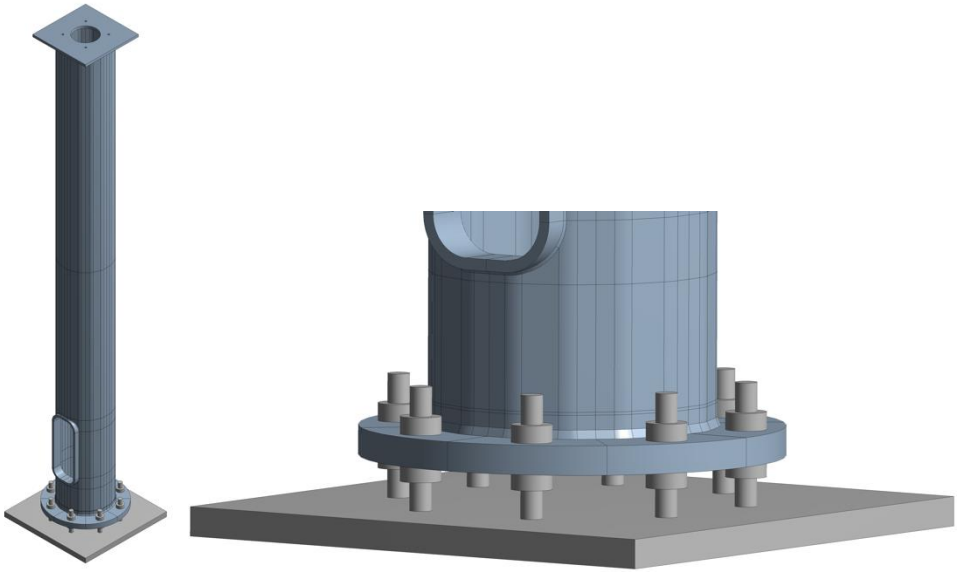

Figure 2.3. Bolted connection and foundation

The friction coefficient is 0.2 for all the contact surfaces between the base plate, bars, and nuts (Oman and Nagode 2017).

In these four specimen models, locations with high stress concentration were expected to be around the base-to-tube connection and the hand hole. In order to have higher accuracy at these locations, the finest meshes were used on the base plate, the hand hole, and the lower region of the tube.

2.2. Static Analysis

Static analysis was conducted by applying a static load at the top surface of the top plate. The bottom surface of the foundation was defined as fixed support. Before studying the stress response of the four different models, the finite element models needed to be verified first. In Roy et al. (2011), strain gauges were installed on specimen Type X to read the stress value around the base-to-tube connection and the hand hole.

Figure 2.4 shows the 11 data points measured by the strain gauges during a static test in Roy et al. (2011), and the simulated stress response of Specimen C from the weld toe of the base-to-tube connection to the hand hole.

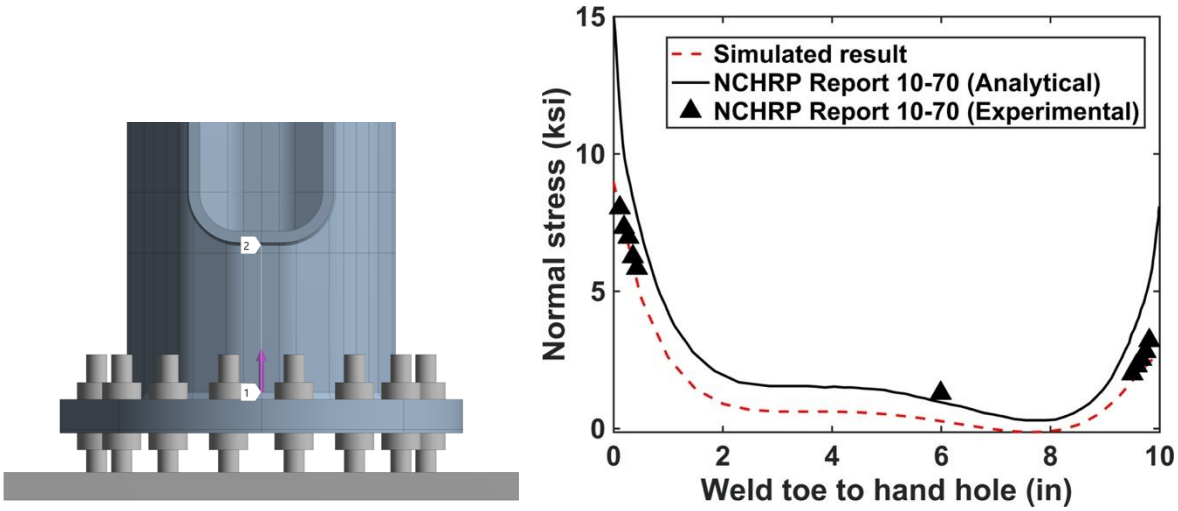

Figure 2.4. Stress response from the weld toe of the base-to-tube connection to the hand hole

The simulated stress response showed strong agreement with the readings from the strain gauges, which indicated that the finite element model was accurately designed and the mesh quality around the location of interests was good enough.

After the verification of the finite element models, a 1 kip static load was applied on each model to compare the stress response at the base. The hand-hole side of the specimens was in tension, and the back side was in compression, named Case 1. Table 2.1 shows the surface normal stress in the vertical direction at the base of Specimen A and Specimen B.

Table 2.1. Surface normal stress at the base of Specimen A and Specimen B

	Specimen A	Specimen B
Hand-hole side	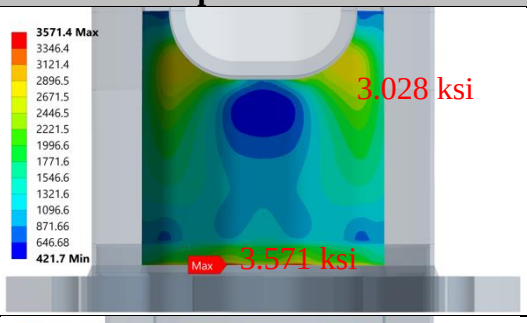	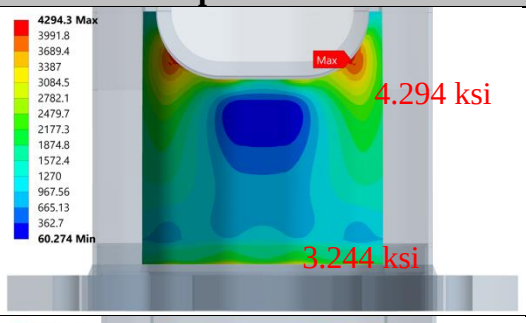
Back side	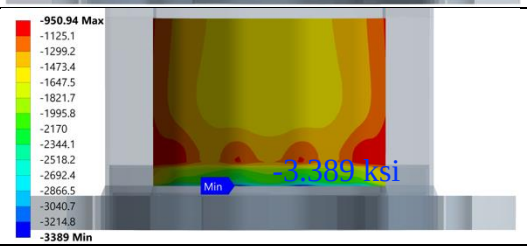	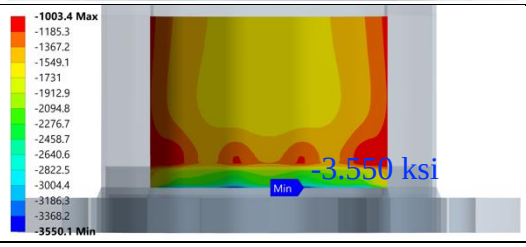

On the hand-hole side, the maximum stress was shown to be at the weld toe of the base-to-tube connection on Specimen A; however, the maximum stress was shown at the bottom corner of the hand hole on Specimen B. This indicates that increasing the opening from 11 in. to 13 in. can result in maximum stress shifts from the base-to-tube connection to the corners of the hand hole. On the back side, since the geometry of the two specimens were identical, the stress responses were also very similar.

Table 2.2 shows the surface normal stress in the vertical direction of Specimen C and Specimen D.

Table 2.2. Surface normal stress at the base of Specimen C and Specimen D

	Specimen C	Specimen D
Hand-hole side	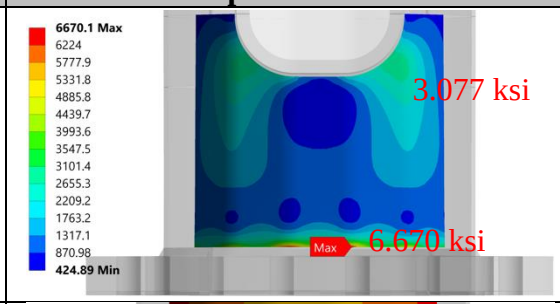	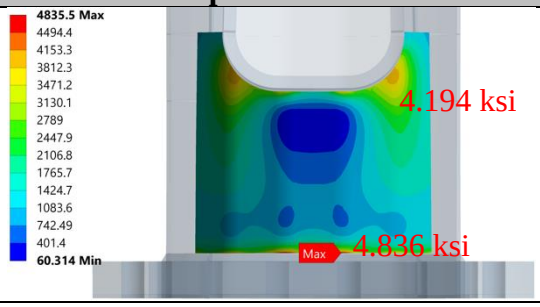
Back side	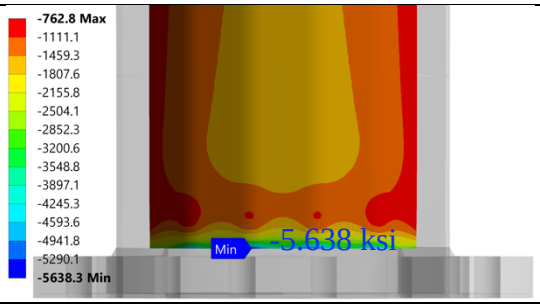	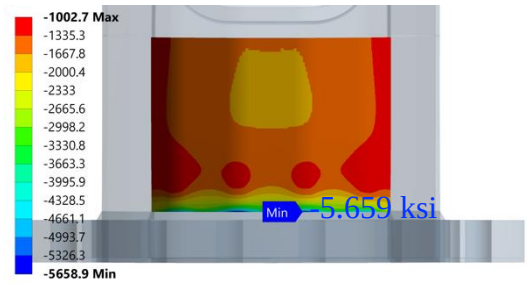

On the hand-hole side, both Specimen C and Specimen D showed the maximum stress at the weld toe of the base-to-tube connection. From a comparison of Specimen C and Specimen D, it was also found that increasing the opening of the hand hole resulted in the increase of stress at the corners of the hand hole. Additionally, there was a significant decrease of stress at the weld toe of the base-to-tube connection when increasing the opening from 11 in. to 13 in. The same thing was also observed in the comparison of Specimen A and Specimen B. Based on these two comparisons, increasing the size of the opening might increase the possibility of fatigue cracks appearing at the corners of the hand hole.

Static analysis was also conducted by applying a 1 kip load in the opposite direction to make the hand-hole side in compression and the back side in tension, named Case 2. Table 2.3 summarizes the results of the static analysis. The stress range (S_r) was defined as the range of the surface normal stress from Case 1 to Case 2.

Table 2.3. Maximum surface normal stress and stress range (S_r) at locations of interests

Stress (ksi)	Base-to-tube connection (hand-hole side)			Base-to-tube connection (back side)			Hand hole corner		
Specimens	Case 1	Case 2	S_r	Case 1	Case 2	S_r	Case 1	Case 2	S_r
A	3.571	-3.285	6.856	-3.389	3.692	7.081	3.028	-3.093	6.121
B	3.244	-2.954	6.198	-3.550	3.858	7.408	4.294	-4.369	8.663
C	6.670	-5.914	12.584	-5.638	6.407	12.045	3.077	-3.160	6.237
D	4.836	-4.836	9.672	-5.659	5.659	11.318	4.194	-4.194	8.388

Finally, Specimen A and Specimen B were used in a fatigue experiment to study the influence of the opening of the hand hole on the fatigue resistance of the high-mast lighting towers. These specimens were selected because according to the finite element analysis, this pair of specimens showed the maximum stress range at different locations. It is believed that fatigue cracks would most likely occur at locations with high stress concentration. Therefore, Specimen A and Specimen B might show fatigue cracks at different locations in the fatigue test, which would provide critical information about the influence of the opening ratio on the fatigue performance. The fatigue experiment is explained in Chapter 3.

3. FATIGUE EXPERIMENT

3.1. Experiment Setup

As described in Chapter 2, Specimen A and Specimen B were selected for fatigue experiment. In total, four test specimens were purchased, two of Specimen A and two of Specimen B. To enhance the efficiency of the fatigue experiment, the experiment setup was the same setup used in Rios (2007) and Stam et al. (2011).

Two test specimens were connected to a loading box, and two ends of the setup were designed as cylinder supports. An actuator was attached to the top of the loading box to provide the fatigue load and create fatigue stress cycles at the base of both specimens. Figure 3.1 shows the model and a photograph of the entire fatigue experiment setup, and Figure 3.2 provides photographs of the details.

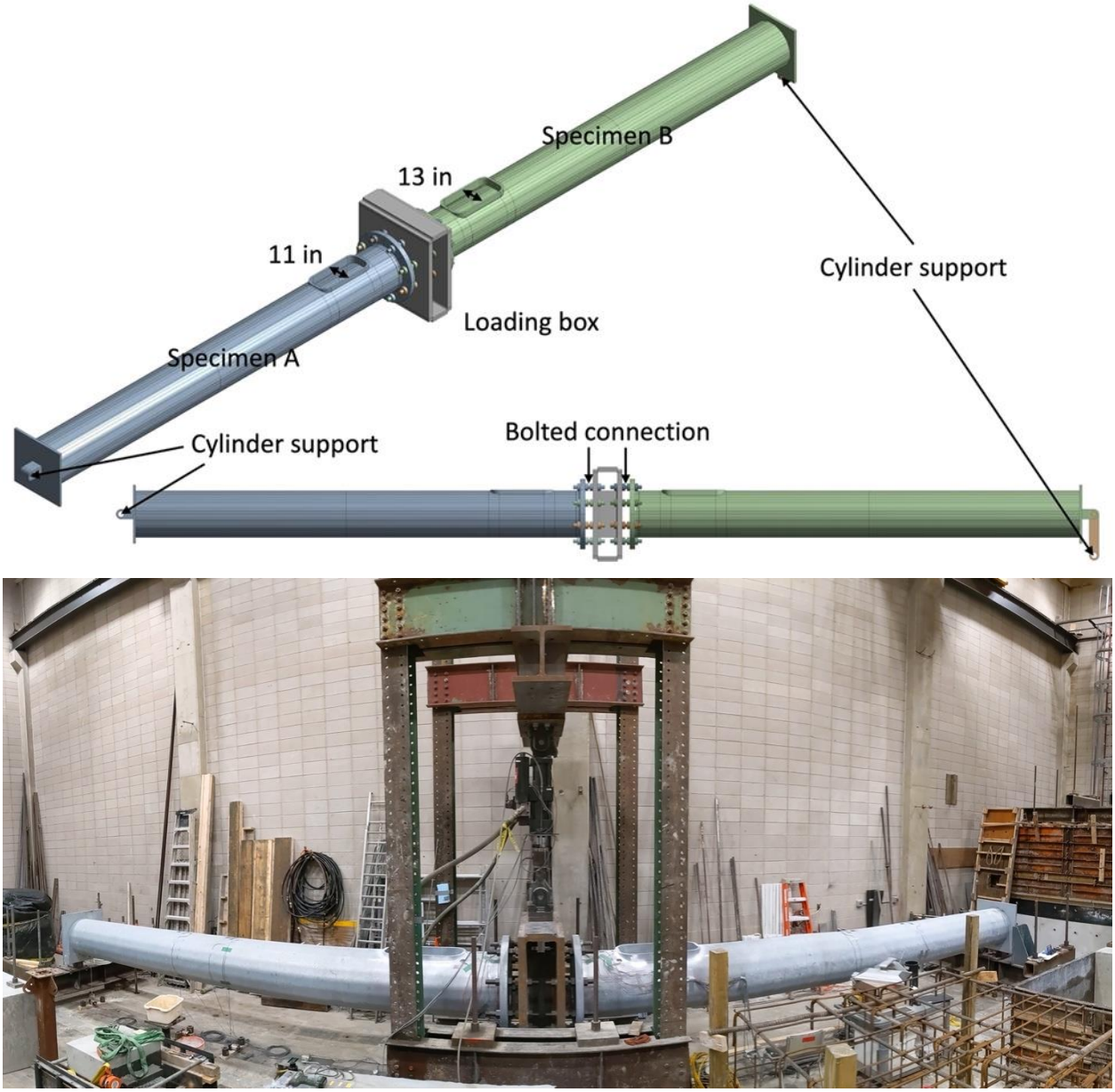

Figure 3.1. Fatigue experiment setup (bottom) and model (top)

(a) (b) (c)

(d) (e) (f)

Figure 3.2. Fatigue experiment setup details

The actuator, Figure 3.2 (a), was installed on a steel frame, Figure 3.2 (f), and connected with the top plate of the loading box. It is capable of both displacement and load control. The load cell of the actuator used MTS Model 661, for which the maximum capacity is 55 kips.

The whole setup can be seen as a simply supported beam. Therefore, the support on one side, Figure 3.2 (b), was designed to rotate freely, and the support on the other side, Figure 3.2 (c), was designed to rotate and move freely in a two-dimensional (2D) plane. To make sure the whole setup can only move in a 2D plane, two triangle stiffener plates were installed on one side of the supports to restrict the movement in the out-of-plane direction (see Figure 3.2 (d)).

The bolted connection, Figure 3.2 (e), between the test specimens and the loading box followed the specification from AASHTO (2015) and the Iowa DOT. Grade 105 threaded bars were used.

Nuts and washers were placed on both sides of the side plates of the loading box and both sides of the base plate of the test specimens. According to the Iowa DOT, the minimum torque requirement for a Grade 105 1.75 in. anchor bolt is 796 ft-lb. A hydraulic wrench was used to tighten the nuts to meet the required torque.

The loading box was composed of five steel plates, which were two side plates, a top plate, a bottom plate, and a middle plate. The plates were fillet welded. There were eight bolt holes on each side plate to connect to the specimens. There were four bolt holes on the top plate to connect to the actuator. See the dimension details in Figure 3.3.

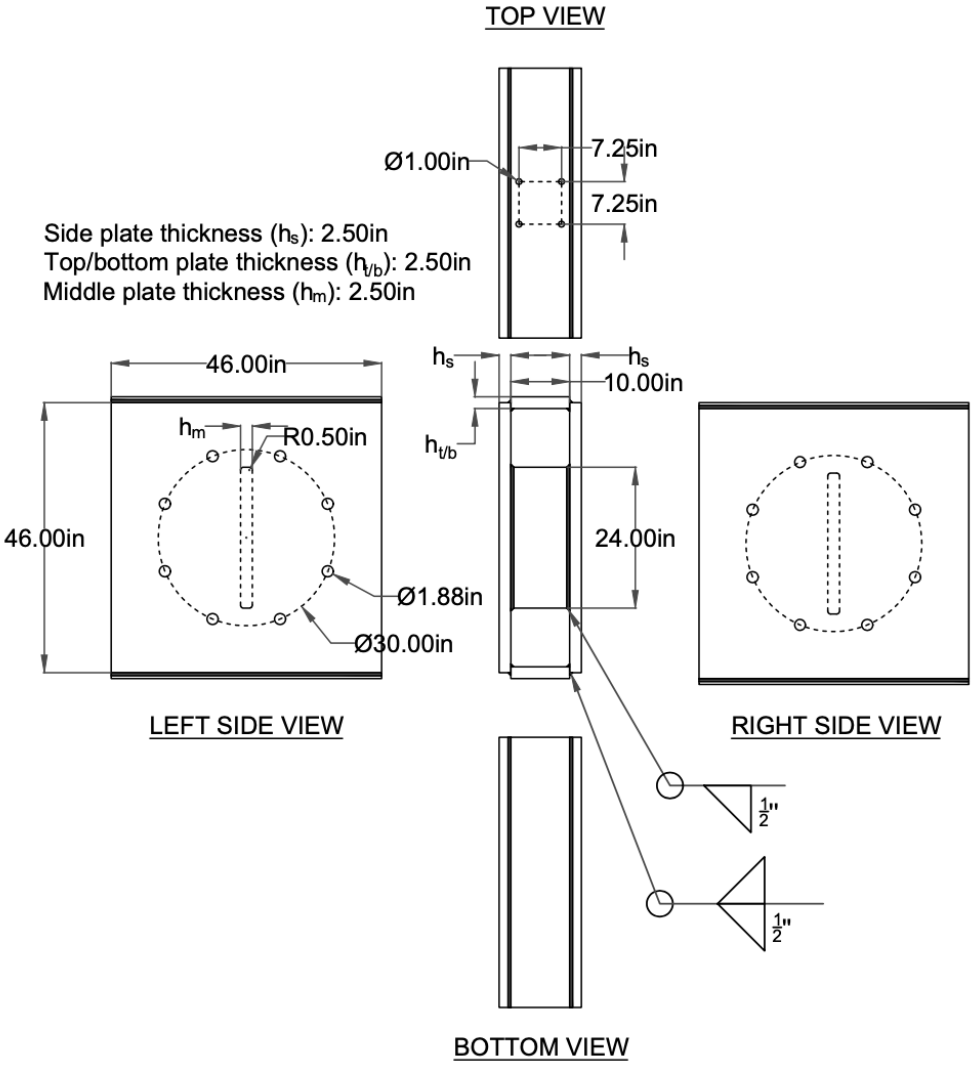

Figure 3.3. Dimension details of loading box

3.2. Instrumentation

Sensors including strain gauges and displacement sensors were used in the experiment, and all the sensors were connected to a data acquisition system to record the data. The details are given in the following subsections.

3.2.1. Strain Gauges

Two types of strain gauges were used: axial gauge and gradient gauge (see Figure 3.4).

Figure 3.4. Axial gauge (left) and gradient gauge (right)

An axial gauge can measure the surface strain in one direction and returns only one strain value. A gradient gauge contains five axial gauges. It also measures the surface strain in one direction but is able to return five strain values along one direction, which gives more information about a location of interest.

Strain gauges were installed for two different purposes. First, strain gauges were installed at hot-spot locations, named hot-spot gauges. Figure 3.5 shows the location and photograph of the hot-spot gauges.

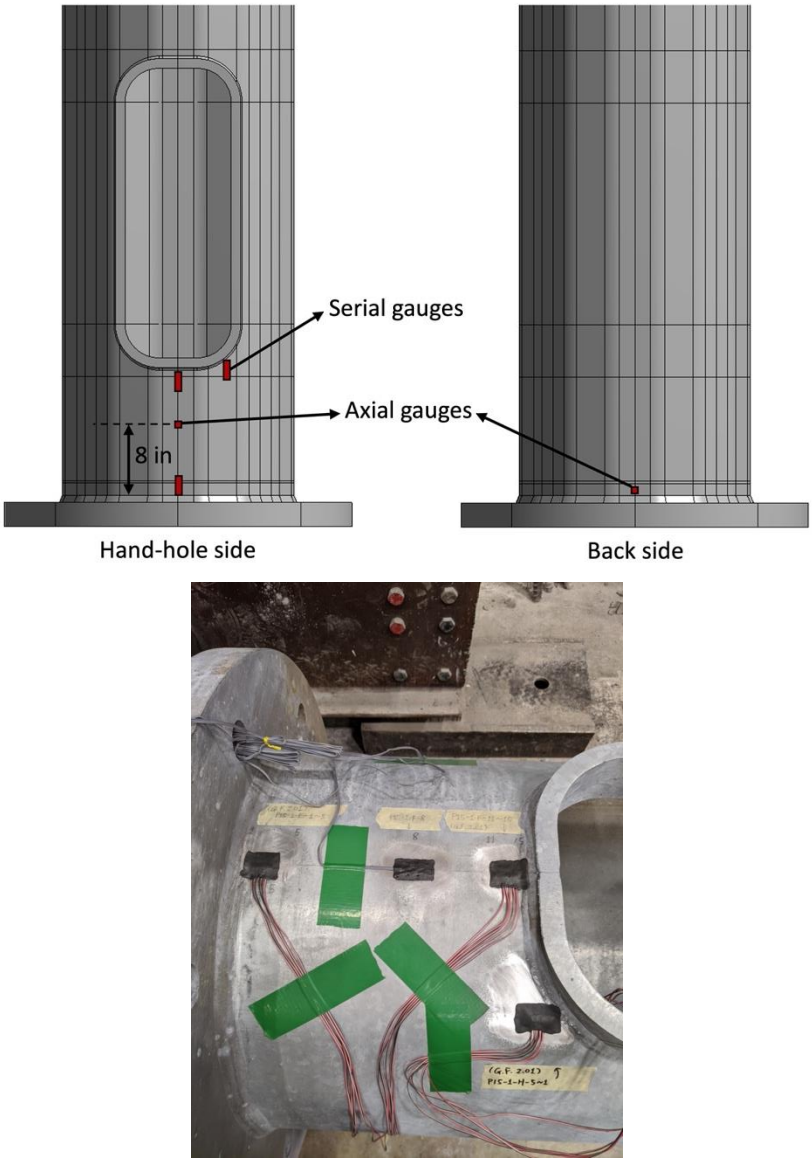

Figure 3.5. Hot-spot gauges (bottom) and locations (top)

Second, four axial gauges were placed on the hand-hole side and the back side at 150 in. and 170 in. from the base plate and named control gauges. See the location and photograph of the control gauges in Figure 3.6.

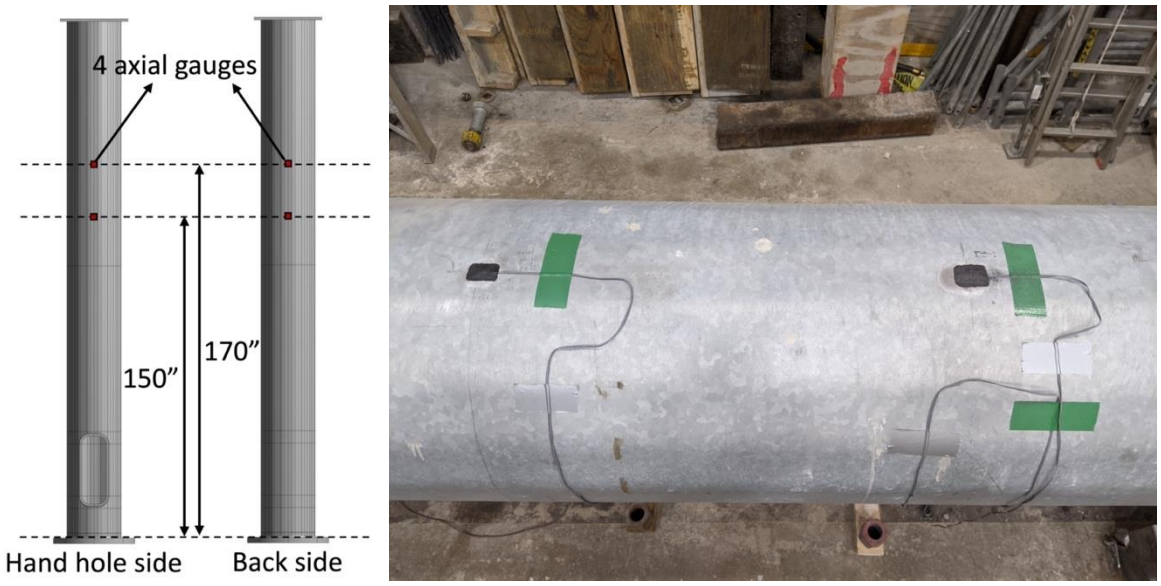

Figure 3.6. Control gauges (right) and locations (left)

Control gauges were placed away from the hand hole to avoid the geometry effect. Therefore, the reading from the control gauges would ideally be very similar to the nominal stress at their locations. Then, the nominal stress at the base-to-tube connection can be calculated by the nominal stress at the control gauges.

The location of the control gauges was decided by a static analysis on finite element models. A 1 kip static load was applied on the top plate. Figure 3.7 shows the surface normal stress and the nominal stress from the top of the hand hole to the top plate.

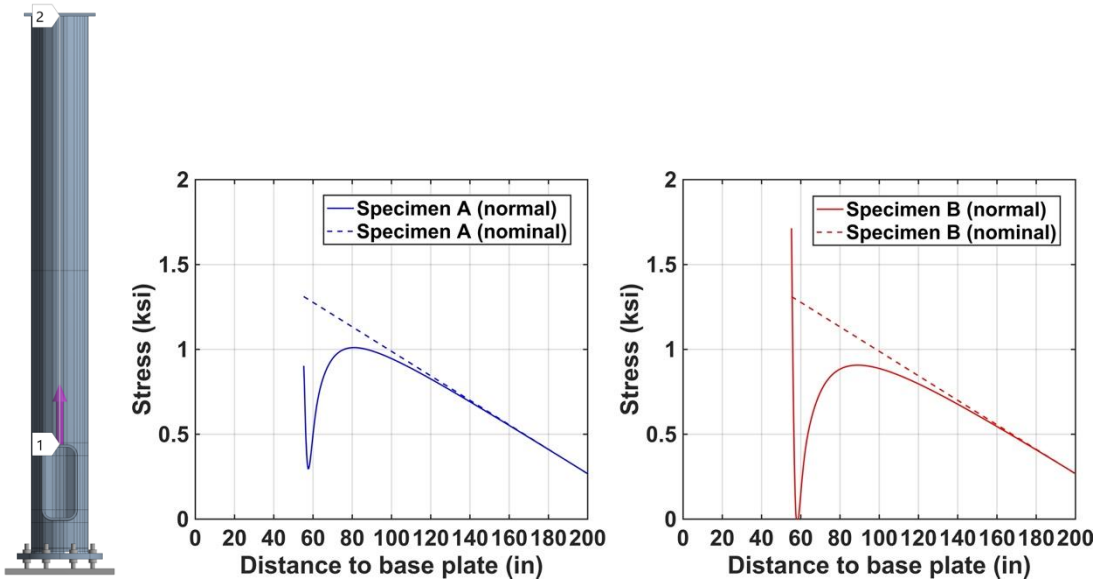

Figure 3.7. Simulated stress response from the top of the hand hole to the top plate

The surface normal stress is nearing the nominal stress when the location is getting away from the geometry effect of the hand hole. It was found that on the hand-hole side, the surface normal stress is almost the same as the nominal stress when the location is at least 140 in. from the base plate. Therefore, the research team decided to place control gauges at 150 in. and 170 in. from the base plate on both the hand-hole side and the back side.

3.2.2. Displacement Sensors

The research team chose to use the HX-PA-10-NJC from UniMeasure for displacement sensors. The measurement range of this sensor is 10 in. Displacement sensors were screwed to a wood brick, and two weights were placed on the wood brick to make it steady (see Figure 3.8).

Figure 3.8. Displacement sensor

To install the displacement sensors, a chain was dropped from the locations of interest and hooked to a ring at the tip of the wire rope (see Figure 3.9 (b) and (c)). A total of 10 displacement sensors were installed to measure the displacement at different locations along the experiment setup (see Figure 3.9 (a)).

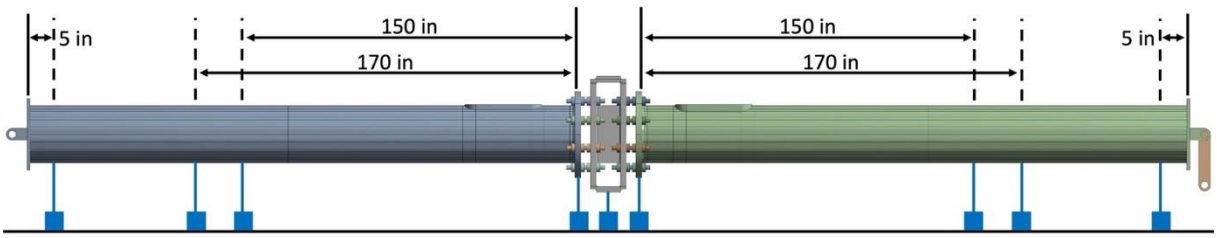

(a)

(b) (c)

Figure 3.9. Locations (top) and displacement sensors (bottom)

There are two sensors at each of the two sides of the bottom plate of the loading box and four sensors on each specimen. At the loading box, two sensors were used to monitor the displacement of the loading box during the fatigue experiment. Also, the values from these two sensors were used to check whether the experiment setup had rotation movement due to the fatigue load.

The displacement data from all the sensors was used to determine the deflected shape of the two specimens, so the second derivative of deflection, bending moment, and nominal stress at different locations could be approximated. The detail calculations are explained in Section 3.4.

3.2.3. Data Acquisition System

The data acquisition system chosen was the Model 5100B Scanner from Vishay Intertechnology (see Figure 3.10).

Figure 3.10. Data acquisition system

All the sensors were connected to the scanners, and the scanners were connected to a computer. A software package called StrainSmart 5000 was installed in the computer and provided a user interface to configure the data from all the sensors. Strain data was recorded in microstrain ($\mu\varepsilon$). Displacement data was recorded in 0.001 in. The displacement and load signals from the actuator were also recorded. During the fatigue experiment, the sampling rate was set to 50 Hz, and the data was recorded for 1 minute in every 15 minutes.

3.3. Experiment Procedures

There was a total of four specimens. Using the experiment setup explained in Section 3.1, Specimen A and Specimen B were tested together, and two fatigue tests were conducted. Before each fatigue test, there was an inspection of the specimens. A dye penetrant test and a magnetic particle test were used to make sure the specimens were in good condition before the fatigue test. Hot-spot locations including the base-to-tube connection and the weld around the hand hole were inspected.

The dye penetrant test typically includes four steps. First, use a cleaner to clean the surface of the test object. Second, spray a dye penetrant on the surface and allow it to sit for 10–30 minutes. Third, wipe the surface clean with a clean towel or cloth. Fourth, spray a developer on the surface and watch whether there's any red indications on the surface. The magnetic particle test is relatively simpler and faster and typically includes three steps. First, clean the surface of the test object. Second, spray a magnetic powder on the surface. Third, apply a magnetic field on the surface and observe whether there's any indications.

After the initial inspection of the specimens, a static test was conducted to determine the required load on the loading box to create the desired stress cycle at the base-to-tube connection. Next, by applying the required load, fully reversed constant-amplitude stress cycles were applied on the

specimens. During the fatigue testing, dye penetrant test and magnetic particle tests were conducted at different numbers of cycles to check the condition of the specimens. Finally, the fatigue test was continued until fatigue failure appeared on the specimens.

An experiment setup model was built in Ansys software to conduct a modal analysis (see Figure 3.11).

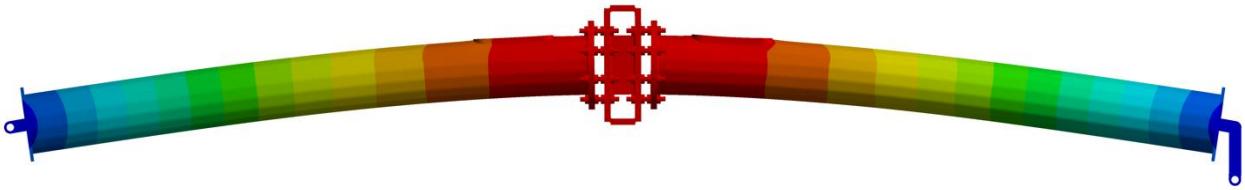

Figure 3.11. The mode shape of the first mode of the fatigue experiment setup

The structural frequency of the first mode of the experiment setup was identified as 4.689 Hz. To avoid resonance during the fatigue test, the frequency of the fatigue load was determined to be lower than 2 Hz. The data sampling rate was then determined to be at least 50 Hz.

For the selection of nominal stress range at the base-to-tube connection in fatigue tests, the research team considered the tests conducted in Roy et al. (2011), where Type XI specimens—which is identical to Specimen A in the present study—were tested with three different nominal stress ranges: 10 ksi, 12 ksi, and 16 ksi. The test results of that study are shown in Figure 129 in Roy et al. (2011). In the present study, a lower nominal stress range, 8 ksi, was selected for the first fatigue test since Specimen B, which has a larger hand hole, and Specimen A were tested at the same time. The plan was to observe whether Specimen A showed a similar fatigue resistance as specimen Type XI and whether Specimen B had a different fatigue resistance. In the second fatigue test, the nominal stress range was set to 16 ksi to evaluate their fatigue resistances at a different level of nominal stress range. Finally, the fatigue resistance of both specimens was determined by AASHTO fatigue category.

According to Roy et al. (2011), fatigue failure is generally defined as a visible through-thickness crack with a minimum of 5 in. (127 mm) in length measured from tip to tip. However, fatigue failure at a tubular connection is defined as half the diameter of the tube, which is equal to 12 in. in this study. The run-out life for an infinite life fatigue test should be taken as: 12.5×10^6 cycles at 16.0 ksi, 7.0×10^6 cycles at 12.0 ksi, 8.2×10^6 cycles at 10.0 ksi, 14.7×10^6 cycles at 7.0 ksi, 20×10^6 cycles at 4.5 ksi, and 20×10^6 cycles at 2.6 ksi.

3.4. Static Test Results

A static test was conducted before the fatigue test to determine the required fatigue load at the loading box.

3.4.1. Determination of Required Fatigue Loads

As mentioned in Section 3.3, the nominal stress range at the base-to-tube connection was set to 8 ksi and 16 ksi for the first and the second fatigue tests, respectively. Fully reversed constant-amplitude stress cycles were applied at the base-to-tube connection. Then, the required loads at the loading box needed to be calculated. Knowing the cross-section property, nominal stress can be simply calculated from bending moment using the following equation.

$$\sigma_{nominal} = \frac{Mc}{I} \quad \textbf{(3.1)}$$

where M is the bending moment, c is the perpendicular distance to the neutral axis, and I is the moment of inertia.

However, because of the design of the experiment setup, the bending moment at the base-to-tube connection cannot be calculated directly from the applied load at the loading box. In this study, stress from hot-spot gauges at the base-to-tube connection was converted to the nominal stress by the identified stress concentration factor. Data from the control gauges and displacement sensors were used to confirm whether the calculated nominal stress at the base-to-tube connection was accurate. Different static loads were applied at the loading box, and a fitting function was built for the relationship between the static load and the nominal stress at the base-to-tube connection. Then, the required loads to create the desired nominal stress at the base-to-tube connection were finally determined.

In this study, different static loads from 11 kips to 25 kips and from -1 kips to -15 kips with an increment of 1 kip were applied at the loading box. Positive load represents upward direction and negative load represents downward direction. In the following tests, three different approaches were used to confirm the required fatigue load.

In the first approach, the stress concentration factor (SCF) at the base-to-tube connection was used to convert the surface stress recorded by the hot-spot gauges at the base-to-tube connection to the nominal stress. In Figure 2.4, the finite element analysis was validated to be able to precisely simulate the stress response near the weld toe of the base-to-tube connection. Therefore, finite element models of Specimen A and Specimen B were used to calculate the SCF at the weld toe of the base-to-tube connection. Static load was applied on the top of the finite element models, and the SCF is the ratio of the surface stress and the nominal stress at the weld toe of the base-to-tube connection. Table 3.1 shows the identified SCF at the weld toe of the base-to-tube connection.

Table 3.1. SCF at the weld toe of the base-to-tube connection

Locations	Hand hole side	Back side
SCF	1.99	2.59

After identifying the SCF at the base-to-tube connection, the surface stress from the hot-spot gauges can be converted to the nominal stress (see some examples in Table 3.2)

Table 3.2. Surface stress (ksi) at the base-to-tube connection to nominal stress (ksi)

Static loads (kips)		**15**	**16**	**17**	**18**	**-8**	**-7**	**-6**	**-5**
Hand-hole side	**Surface stress**	10.77	11.91	13.05	14.16	-13.71	-12.57	-11.43	-10.35
	Nominal stress	**5.41**	**5.98**	**6.55**	**7.11**	**-6.89**	**-6.31**	**-5.74**	**-5.20**
Back side	**Surface stress**	-14.01	-15.48	-16.92	-18.36	18.12	16.59	15.06	13.59
	Nominal stress	**-5.41**	**-5.98**	**-6.53**	**-7.09**	**6.99**	**6.40**	**5.81**	**5.25**

It can be seen that the calculated nominal stress at the hand-hole side and at the back side have a similar value with opposite sign, which indicates the identified SCF at the base-to-tube connection could be accurate.

In the second approach, control gauges read the nominal stress at their locations, which was used to predict the nominal stress at the base-to-tube connection. Two stress values recorded by two control gauges at 150 in. and 170 in. from the base plate were used to calculate the bending moments at these two locations by using equation 3.1. The bending moment at the cylinder support was assumed to be zero. Using these three data, the bending moment along the specimen can be approximated by the least-square method. The bending moment function was approximated by a second-order polynomial function.

Table 3.3 shows the recorded stress at the control gauges and the predicted nominal stress at the base-to-tube connection when applying different static loads.

Table 3.3. Surface stress (ksi) from control gauges to nominal stress (ksi) at the base-to-tube connection

Static loads (kips)		15	16	17	18	-8	-7	-6	-5
Control gauge at 150 in.	Hand-hole side	3.45	3.81	4.17	4.50	-4.80	-4.47	-4.14	-3.78
	Back side	-3.45	-3.84	-4.23	-4.53	4.83	4.47	4.08	3.72
Control gauge at 170 in.	Hand-hole side	2.76	3.06	3.36	3.63	-3.84	-3.54	-3.24	-2.97
	Back side	-2.70	-3.03	-3.30	-3.57	3.72	3.45	3.18	2.88
Nominal stress at the base-to-tube connection		**5.02**	**5.58**	**6.11**	**6.59**	**6.98**	**6.47**	**5.95**	**5.43**

As shown in Table 3.3, the predicted nominal stress at the base-to-tube connection is similar to the nominal stress calculated by the SCF at the base-to-tube connection in Table 3.2. Therefore, the relationship between static loads and the nominal stress at the base-to-tube connection from the first approach was determined to be accurate.

In the third approach, displacement data from the displacement sensors were used to approximate the deflection function of the specimens. The deflection function was approximated by a third-order polynomial function. The second derivative of deflection was calculated from the deflection function. Then, the bending moment along the specimen was calculated by equation 3.2, and the nominal stress at the base-to-tube connection was determined.

$$\boldsymbol{M(x) = EIy''(x)} \quad \textbf{(3.2)}$$

where E is the modulus of elasticity of structural steel, which equals to 30×10^6 (psi), and I is the moment of inertia.

Table 3.4 shows the displacement data at different static loads and the predicted nominal stress at the base-to-tube connection.

Table 3.4. Displacement data (in.) to nominal stress (ksi) at the base-to-tube connection

Static loads (kips)		15	16	17	18	-8	-7	-6	-5
Distance to base plate	223 in.	0.069	0.075	0.083	0.089	-0.076	-0.071	-0.065	-0.060
	170 in.	0.242	0.266	0.293	0.317	-0.308	-0.285	-0.258	-0.239
	150 in.	0.314	0.347	0.379	0.411	-0.417	-0.386	-0.353	-0.325
	0 in.	0.620	0.682	0.750	0.809	-0.837	-0.776	-0.709	-0.657
Nominal stress at the base-to-tube connection		**5.30**	**5.91**	**6.40**	**7.02**	**6.71**	**6.17**	**5.58**	**5.09**

As shown in Table 3.4, the predicted nominal stress at the base-to-tube connection is similar to the nominal stress calculated by the SCF at the base-to-tube connection in Table 3.2. Therefore, the relationship between static loads and the nominal stress at the base-to-tube connection from the first approach was confirmed again.

At this point, the relationship between the static load and the nominal stress at the base-to-tube connection found by using the stress concentration factor in the first approach has been validated by the data from the control gauges and the displacement sensors. Finally, the relationship between the static load and the nominal stress at the base-to-tube connection was approximated by a polynomial function (see Figure 3.12).

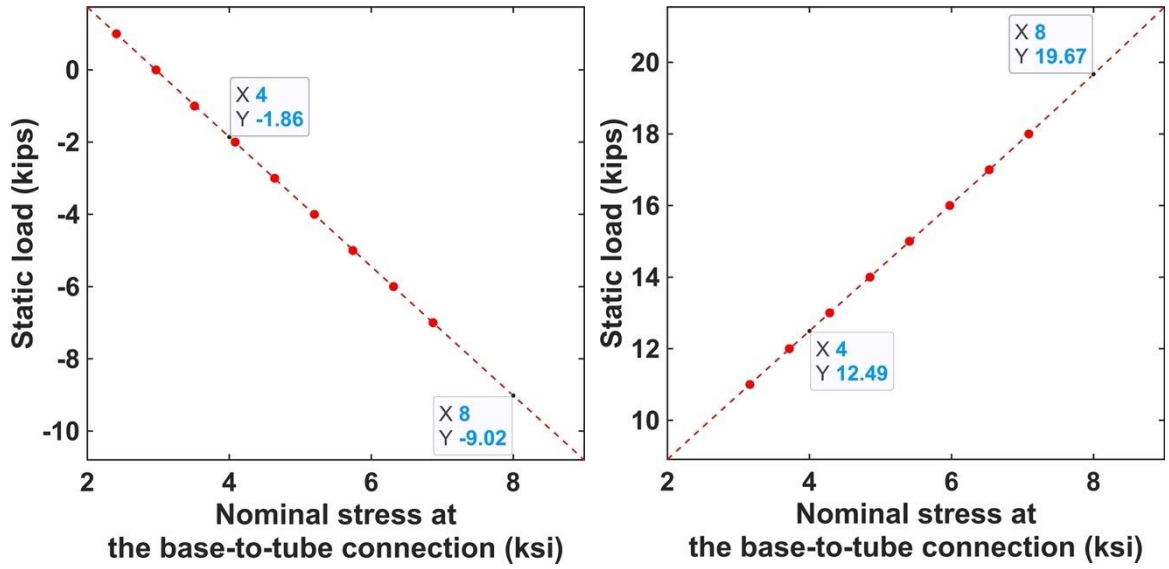

Figure 3.12. Static load at the loading box vs. nominal stress at the base-to-tube connection

The required fatigue loads were finally determined as 12.5 kips and -1.9 kips to create the nominal stress range of 8 ksi at the base-to-tube connection and 19.7 kips and -9.0 kips to create the nominal stress range of 16 ksi at the base-to-tube connection.

3.5. Fatigue Test Results

3.5.1. Initial Inspection of Test Specimens

As mentioned in Section 3.3, a dye penetrant test and a magnetic particle test were conducted on the specimens before the fatigue test to examine whether the specimens were in good condition. Figure 3.13 and Figure 3.14 show the results of the initial dye penetrant test.

(a) Base-to-tube connection

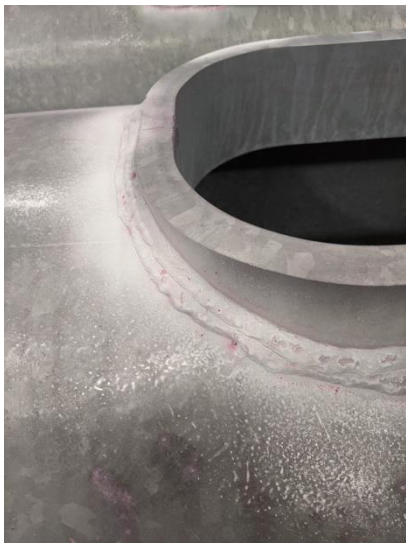

(b) Hand hole top left corner

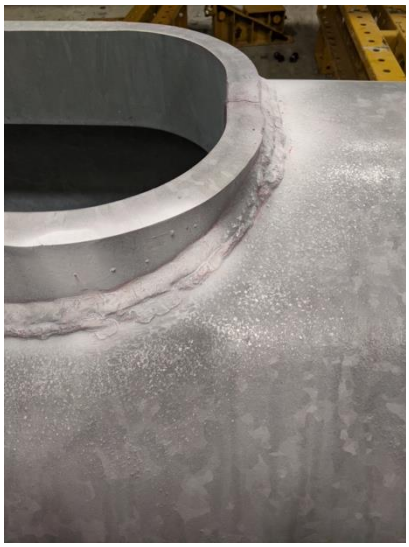

(c) Hand hole top right corner

(d) Hand hole bottom left corner

(e) Hand hole bottom right corner

Figure 3.13. Initial dye penetrant test on Specimen A

(a) Base-to-tube connection

(b) Hand hole top left corner

(c) Hand hole top right corner

(d) Hand hole bottom left corner

(e) Hand hole bottom right corner

Figure 3.14. Initial dye penetrant test on Specimen B

Both tests showed no indications on the hot-spot locations, which indicates the specimens were in good condition before the fatigue test.

3.5.2. First Fatigue Test

In the first fatigue test, Specimen A-1 and Specimen B-1 were connected to the loading box and tested together. The stress range at the base-to-tube connection was set to 8 ksi, the fatigue load was a sinusoidal load with the high end at 12.5 kips and the low end at -1.9 kips, and the load frequency was set to 0.6 Hz. Dye penetrant tests and magnetic particle tests were conducted at

650,000, 850,000, and 1,000,000 cycles to inspect the condition of the specimens. The test was stopped at 1,000,000 cycles.

On Specimen A-1, no indications were found at the base-to-tube connection and the hand-hole-to-tube connection at 1,000,000 cycles from both the dye penetrant test and magnetic particle test. See Figure 3.15 for the results of the dye penetrant test on Specimen A-1 at 1,000,000 cycles.

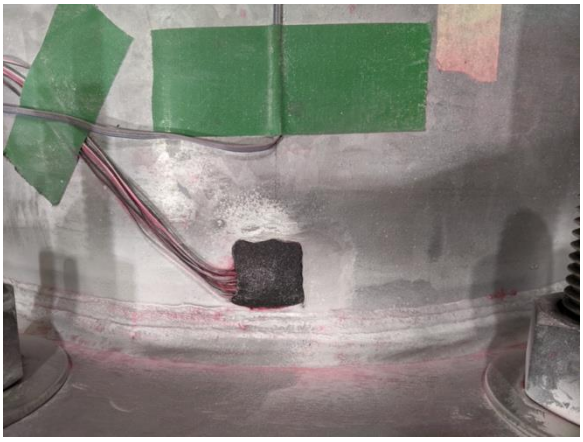

(a) Hand-hole side of the base-to-tube connection

(b) Back side of the base-to-tube connection

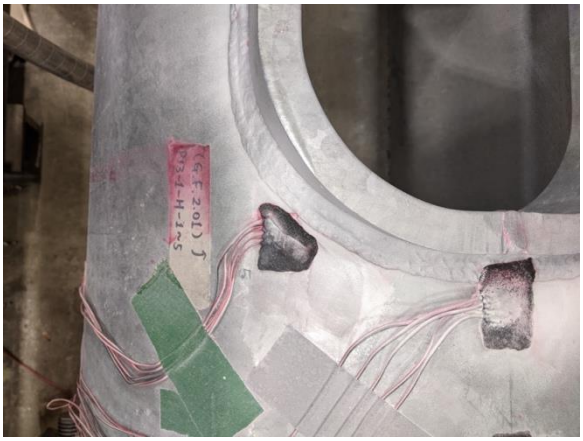

(c) Left bottom corner of the hand hole

(d) Right bottom corner of the hand hole

Figure 3.15. Dye penetrant test result of Specimen A-1

On Specimen B-1, small red indications were found at the bottom corners of the hand hole, and no red indications were found at the base-to-tube connection from the dye penetrant test at 1,000,000 cycles (see Figure 3.16).

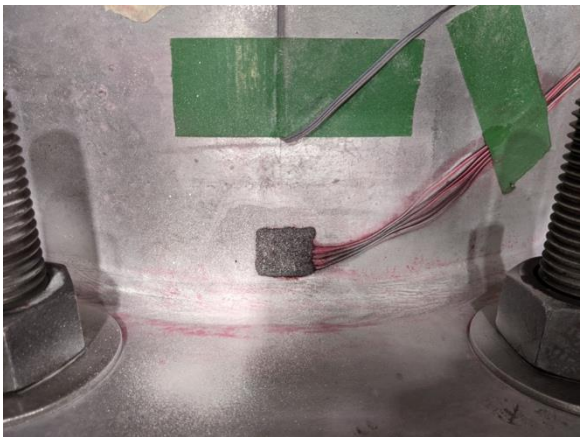

(a) Hand-hole side of the base-to-tube connection

(b) Back side of the base-to-tube connection

(c) Left bottom corner of the hand hole

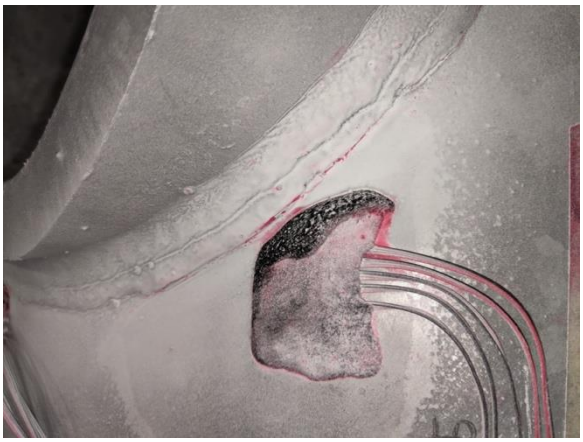

(d) Right bottom corner of the hand hole

Figure 3.16. Dye penetrant test result of Specimen B-1

However, the magnetic particle test at 1,000,000 cycles showed no indication at both the bottom corners of the hand hole and the base-to-tube connection. Also, from the readings of the hot-spot gauges, no obvious change was found in the stress range as the number of cycles reached 1,000,000 (see Figure 3.17).

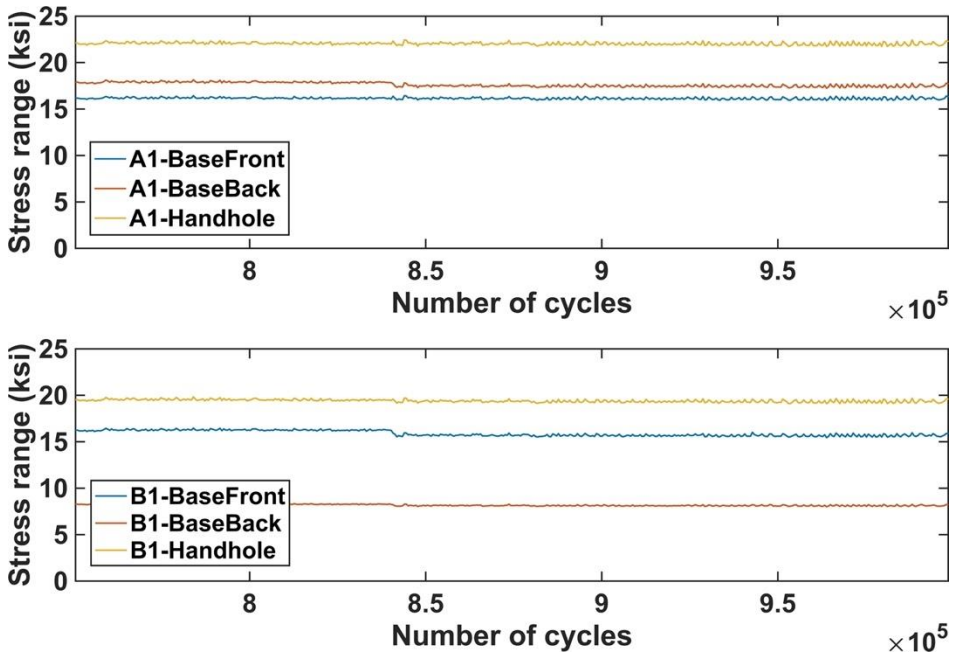

Figure 3.17. Stress ranges from hot-spot gauges of Specimen A-1 and Specimen B-1

Therefore, the small red indications from the dye penetrant test might be due to the poor cleaning of the surface and might not be through-thickness fatigue cracks.

3.5.3. Second Fatigue Test

In the second fatigue test, Specimen A-2 and Specimen B-2 were connected to the loading box and tested together. The stress range at the base-to-tube connection was set to 16 ksi, the fatigue load was a sinusoid load with the high end at 19.7 kips and the low end at -9 kips, and the load frequency was set to 0.6 Hz. Dye penetrant tests and magnetic particle tests were conducted at 100,000 and 115,000 cycles to inspect the condition of the specimens. The test was stopped at 115,000 cycles because the vibration amplitude at the loading box increased more than 10%.

On Specimen A-2, no indications were found at the base-to-tube connection and the hand-hole-to-tube connection from both the dye penetrant test and magnetic particle test at 115,000 cycles. However, the readings from the hot-spot gauges at the base-to-tube connection showed a slightly decaying trend at about 110,000 cycles (see Figure 3.18).

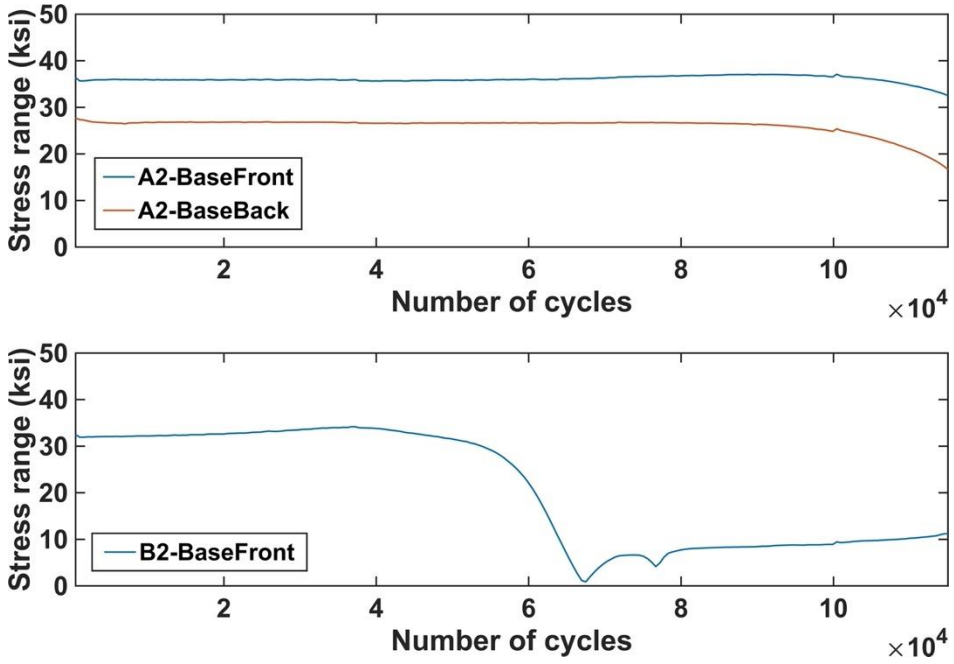

Figure 3.18. Stress ranges from the hot-spot gauges of Specimen A-2 and Specimen B-2

This might indicate that a fatigue crack might be about to occur at the base-to-tube connection on Specimen A-2.

On Specimen B-2, a small indication with a length of about 4 in. at the hand-hole side of the base-to-tube connection was found by the magnetic particle test at 100,000 cycles (see Figure 3.19 (a)).

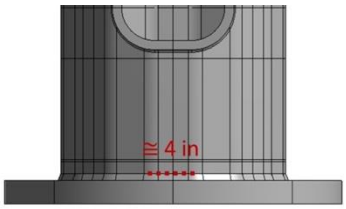

(a) 100,000 cycles

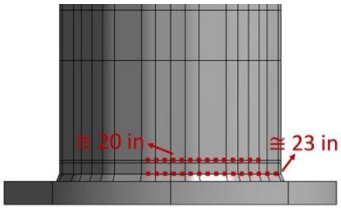

(b) 115,000 cycles

Figure 3.19. Inspection result of Specimen B-2 at (a) 100,000 cycles and (b) 115,000 cycles

A large fatigue crack with a length of more than 20 in. at the back side of the base-to-tube connection was observed at 115,000 cycles. A fatigue crack with a length of more than 20 in. at the top of the backing ring was also observed (see Figure 3.19 (b)). In Figure 3.18, the hot-spot gauge at the hand-hole side of the base-to-tube connection showed that the stress range decreased dramatically at about 60,000 cycles, which indicates that the fatigue crack might have occurred at somewhere between 60,000 and 100,000 cycles.

3.5.4. Summary of the Fatigue Tests

Figure 3.20 shows the fatigue test result of Specimen A-1 and Specimen A-2.

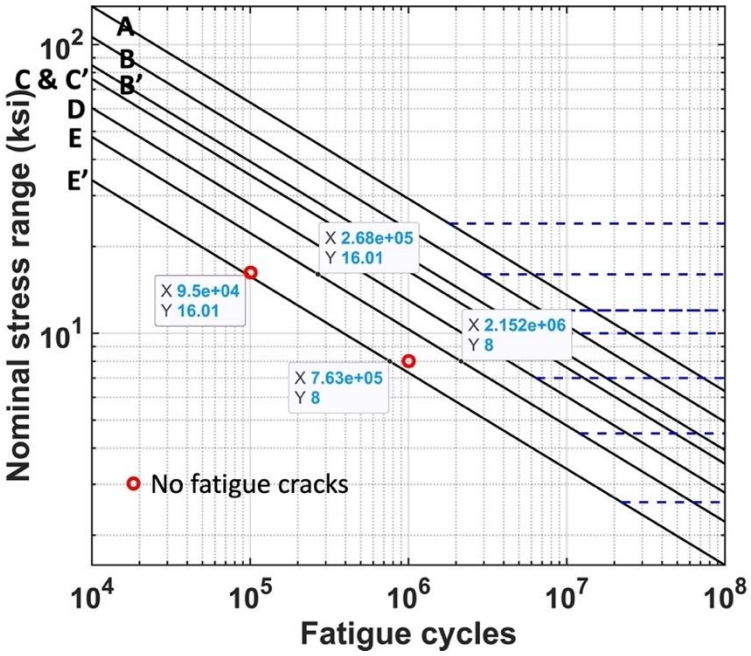

Figure 3.20. Fatigue test result of Specimen A

The base-to-tube connection of Specimen A was shown to have a fatigue resistance for finite life higher than Category E′. Also, according to the decaying trend of the stress range at the base-to-tube connection observed at around 110,000 cycles, the base-to-tube connection might have a fatigue resistance for finite life lower than Category E. The test result of specimen Type XI in Roy et al. (2011) also showed that the fatigue resistance of its base-to-tube connection was between Category E′ and Category E. No cracks were found around the hand-hole-to-tube connection; therefore, the fatigue resistance for finite life of the hand-hole-to-tube connection of Specimen A was identified as higher than Category E′.

Figure 3.21 shows the fatigue test result of Specimen B-1 and Specimen B-2.

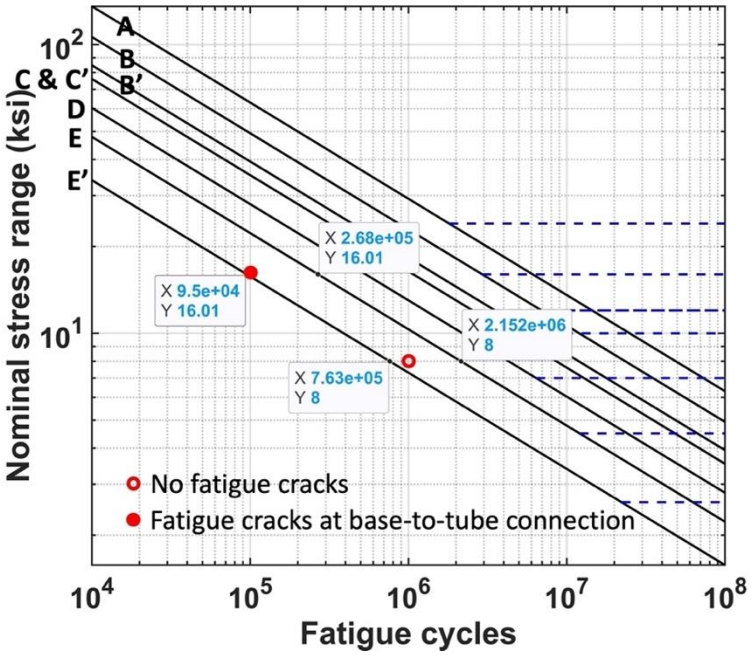

Figure 3.21. Fatigue test result of Specimen B

The base-to-tube connection of Specimen B was shown to have a fatigue resistance for finite life near the lower limit of Category E′. No cracks were found around the hand-hole-to-tube connection; therefore, the fatigue resistance for finite life of the hand-hole-to-tube connection was identified as higher than Category E′.

4. PARAMETRIC STUDY ON OPENING RATIO TO FATIGUE RESISTANCE

This research aims to study the influence of the opening size of the hand hole on the fatigue resistance of a high-mast lighting tower. The parametric study began with simulating the stress response at the pole base for pole models with different opening sizes, and then the study on the opening size to the fatigue resistance could be conducted based on the results from the fatigue experiment.

4.1. Opening Ratio to the Stress Response at the Pole Base

In Section 2.2, four pole models were studied to determine the specimens for the fatigue experiment. In this section, additional pole models were built to study the relationship between the opening ratio and the stress response at the pole base. A total of 16 models of specimen Type X and Type XI with different opening ratios were made. A 1 kip static load was applied at the top plate, and the local maximum normal stress at the front side (hand-hole side) and back side of the base-to-tube connection and at the hand hole corners was recorded.

Figure 4.1 shows the maximum normal stress at the pole base of the models with different opening ratios.

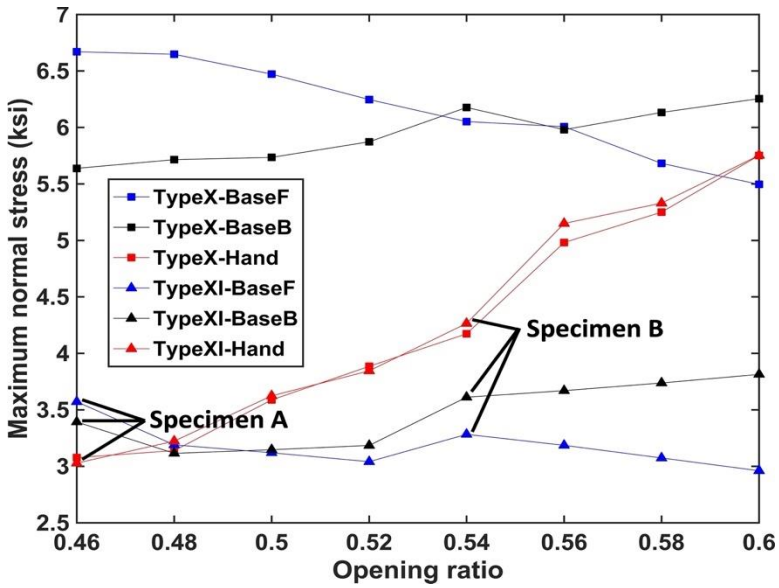

Square markers represent the results of specimen Type X, and triangle markers represent the results of specimen Type XI. Blue represents the stress at the front side of the base-to-tube connection, black represents the stress at the back side of the base-to-tube connection, and red represents the stress at the hand hole corners.

Figure 4.1. Maximum normal stress at the pole base vs. opening ratio

Several things can be observed in Figure 4.1.

First, the stress values at the hand hole corner of specimen Type X and specimen Type XI were very similar, which means different designs of the base-to-tube connection do not have much influence on the stress response around the hand hole.

Second, specimen Type X generally had higher stress at the base-to-tube connection than at the hand hole corners when the opening ratio is smaller than 0.58. Based on this result, specimen Type X might have a higher chance of having fatigue cracks at the base-to-tube connection. Specimen Type X in Roy et al. (2011), which had an opening ratio of 0.46, showed fatigue cracks at the base-to-tube connection and no cracks around the hand hole during the previous fatigue experiment. Similarly, specimen Type XI in Roy et al. (2011), which had an opening ratio of 0.46 and is identical to Specimen A of the present study, was tested in the previous fatigue experiment. The result also showed that fatigue cracks occurred at the base-to-tube connection and no cracks were found around the hand hole. From the stress response in Figure 4.1 and the observations from the previous fatigue experiment, it seems that fatigue cracks might occur at the location with the highest stress.

Third, specimen Type XI generally showed lower stress at the base-to-tube connection than at the hand hole corners when the opening ratio is larger than 0.48. This might be because the backing ring increases the wall thickness at the base-to-tube connection and lowers the stress. Based on the hypothesis mentioned previously, specimen Type XI might have a higher chance of observing fatigue cracks around the hand hole at the base-to-tube connection when the opening ratio is larger than 0.48. This hypothesis can be examined through the fatigue test on Specimen B, which had an opening ratio of 0.54, and is discussed in Section 4.2.

4.2. Opening Ratio to the Fatigue Resistance of High-Mast Lighting Towers

In the present study, two fatigue tests were conducted. In the first fatigue test, no fatigue cracks were found on both Specimen A-1 and Specimen B-1 after the test was stopped at 1,000,000 cycles. In the second fatigue test, fatigue cracks were observed at the base-to-tube connection of Specimen B-2, and no fatigue cracks were found on Specimen A-2. The fatigue resistance for finite life of the base-to-tube connection of Specimen A was identified as higher than Category E′ and possibly lower than Category E. The fatigue resistance for finite life of the base-to-tube connection of Specimen B was identified as near the lower limit of Category E′. Therefore, the fatigue resistance of Specimen A is higher than the fatigue resistance of Specimen B.

Based on this result, it can be inferred that increasing the opening ratio from 0.46 to 0.54 can result in a decrease of fatigue resistance of the base-to-tube connection. In Figure 4.1, it can be seen that there is a slightly increasing trend of stress at the back side of the base-to-tube connection as the opening ratio increases, which might relate to the decrease of fatigue resistance at the base-to-tube connection.

Also, in Section 4.1, based on the finite element analysis and the results from the previous fatigue experiment, a hypothesis was proposed that the fatigue crack on a high-mast pole specimen might occur at the location with the highest stress response. On Specimen B, both the hot-spot gauges and the finite element analysis confirmed that the stress at the hand hole corners

is higher than the stress at the weld toe of the base-to-tube connection. It was expected that a fatigue crack might occur at the hand hole corners prior to the base-to-tube connection. However, in the second fatigue test, a fatigue crack was first observed at the base-to-tube connection, and no cracks were found around the hand hole corners after the test was terminated at 115,000 cycles. Therefore, fatigue cracks on a pole specimen might not occur at the location with the highest stress response. There might be other factors such as the geometry near the discontinuities to determine the location of fatigue cracks.

5. CONCLUSIONS AND FUTURE WORK

In this study, high-mast lighting pole specimens with two different opening ratios of the hand hole were fatigue tested to study the influence that the opening ratio has on fatigue resistance. The findings of this study and potential future work are discussed in this chapter.

The findings of this study are as follows:

- First, the fatigue resistance of the base-to-tube connection decreased as the opening ratio of the hand hole increases. Specimen A had an opening ratio of 0.46, and the fatigue resistance of its base-to-tube connection was determined to be higher than Category E′ and possibly lower than Category E. Specimen B had an opening ratio of 0.54, and the fatigue resistance of its base-to-tube connection was determined to be near the lower limit of Category E′. From the parametric study, a slightly increasing trend of stress at the base-to-tube connection was found as the opening ratio increases. This could be the reason that fatigue resistance decreases at the base-to-tube connection.

- Second, the fatigue resistance of the hand-hole-to-tube connection might be higher than the base-to-tube connection, as no fatigue cracks were observed around both larger and smaller hand holes in both fatigue tests.

- Third, the location of fatigue cracks on a high-mast pole specimen might not completely relate to the stress response, as fatigue cracks were only observed at the base-to-tube connection. However, the stress response at the base-to-tube connection was lower than the stress response at the hand hole corners. There might be other factors such as the geometry near the discontinuities that determine where a fatigue crack will occur on a pole specimen.

Recommendations for future work include the following:

- Only four specimens were tested to determine their fatigue resistance in this study. Tests on additional specimens of each type are needed to identify their fatigue resistance category and scalar more precisely.

- Specimens with only two different opening ratios of the hand hole were tested in this study. Additional tests on different types of specimens with different opening ratios are required to develop the relationship between the opening ratio and fatigue resistance to determine the appropriate opening size based on the required fatigue resistance.

REFERENCES

AASHTO. 2015. *LRFD Specifications for Structural Supports for Highway Signs, Luminaires, and Traffic Signals*. American Association of State and Highway Transportation Officials, Washington, DC.

Ahearn, E. B. and J. A. Puckett. 2010. *Reduction of Wind-Induced Vibrations in High-Mast Light Poles*. University of Wyoming, Laramie, WY.

Caracoglia, L. and N. P. Jones. 2004. *Analysis of Light Pole Failures in Illinois*. University of Illinois at Urbana-Champaign, Urbana, IL.

Chang, B., M. Neill, R. Issa, and A. Miller, A. 2014. Development of Wind Vortex Shedding Coefficients for a Multisided Cylinder Structure. *Wind and Structures,* Vol. 18, No. 2, pp. 181–194.

Dexter, R. J. 2004. *Investigation of Cracking of High-Mast Lighting Towers*. Final Report for the Iowa Department of Transportation, Ames, IA.

Goode, J. S. and J. W. van de Lindt. 2006. Development of a Reliability-Based Design Procedure for High-Mast Lighting Structural Supports in Colorado. Structures Congress 2006. May 18–21, St. Louis, MO.

Luo, Y., Y. Wang, J. Xie, C. Yang, and Y. Zheng. 2017. Aero-Elastic Wind Tunnel Test of a High Lighting Pole. *Wind and Structures,* Vol. *25*, No. 1, pp. 1–24.

Oman, S. and M. Nagode. 2017. Bolted Connection of an End-Plate Cantilever Beam: The Distribution of Operating Force. *Strojniski Vestnik/Journal of Mechanical Engineering*, Vol. 63, No. 11, pp. 617–627.

Phares, B. M., P. P. Sarkar, T. J. Wipf, and B. Chang. 2007. *Development of Fatigue Design. Procedures for Slender, Tapered Support Structures for Highway Signs, Luminaries, and Traffic Signals Subjected to Wind-Induced Excitation from Vortex Shedding and Buffeting*. Midwest Transportation Center, Institute for Transportation, Iowa State University, Ames, IA. https://intrans.iastate.edu/app/uploads/2018/03/Phares_HMLP_final.pdf.

Rios, C. A. 2007. *Fatigue Performance of Multi-Sided High-Mast Lighting Towers*. MS thesis. University of Texas at Austin, TX.

Roy, S., Y. C. Park, R. Sause, J. W. Fisher, and E. J. Kaufmann. 2011. *NCHRP Web-Only Document 176: Cost-Effective Connection Details for Highway, Luminaire, and Traffic Signal Structures*. National Cooperative Highway Research Program, Washington, DC.

Schlatter, C. 2017. *Fatigue Behavior of the Reinforced Electrical Access*. MS thesis. University of Akron, OH.

Stam, A. P., N, Richman, P. Charles, C. Rios, T. Anderson, and K. H. Frank. 2011. *Fatigue Life of Steel Base Plate to Pole Connections for Traffic Structures*. Center for Transportation Research, University of Texas at Austin, TX.

THE INSTITUTE FOR TRANSPORTATION IS THE FOCAL POINT FOR TRANSPORTATION AT IOWA STATE UNIVERSITY.

InTrans centers and programs perform transportation research and provide technology transfer services for government agencies and private companies;

InTrans contributes to Iowa State University and the College of Engineering's educational programs for transportation students and provides K–12 outreach; and

InTrans conducts local, regional, and national transportation services and continuing education programs.

IOWA STATE UNIVERSITY

Visit **InTrans.iastate.edu** for color pdfs of this and other research reports.